Methods

Connecting active to passive fluorescence with photosynthesis: a method for evaluating remote sensing measurements of Chl fluorescence

Troy S. Magney[1], Christian Frankenberg[1,2], Joshua B. Fisher[1], Ying Sun[1,3], Gretchen B. North[4], Thomas S. Davis[5], Ari Kornfeld[6] and Katharina Siebke[7]

[1]Jet Propulsion Laboratory, California Institute of Technology, Pasadena, CA 91109, USA; [2]Division of Geological and Planetary Sciences, California Institute of Technology, Pasadena, CA 91125, USA; [3]School of Integrative Plant Science, Soil and Crop Sciences Section, Cornell University, Ithaca, NY 14853, USA; [4]Biology Department, Occidental College, Los Angeles, CA 90041, USA; [5]Forest and Rangeland Stewardship, Colorado State University, Fort Collins, CO 80523, USA; [6]Department of Global Ecology, Carnegie Institution for Science, Stanford, CA 94305, USA; [7]Heinz Walz GmbH, Eichenring 6, Effeltrich 91090, Germany

Author for correspondence:
Troy S. Magney
Tel: +1 818 364 3266
Email: Troy.S.Magney@jpl.nasa.gov

Received: *2 February 2017*
Accepted: *14 May 2017*

New Phytologist (2017)
doi: 10.1111/nph.14662

Key words: Chl fluorescence, fluorescence spectra, gross primary production, leaf level, photosynthesis, pulse-amplitude modulation (PAM), remote sensing, solar induced Chl fluorescence (SIF).

Summary

- Recent advances in the retrieval of Chl fluorescence from space using passive methods (solar-induced Chl fluorescence, SIF) promise improved mapping of plant photosynthesis globally. However, unresolved issues related to the spatial, spectral, and temporal dynamics of vegetation fluorescence complicate our ability to interpret SIF measurements.
- We developed an instrument to measure leaf-level gas exchange simultaneously with pulse-amplitude modulation (PAM) and spectrally resolved fluorescence over the same field of view – allowing us to investigate the relationships between active and passive fluorescence with photosynthesis.
- Strongly correlated, slope-dependent relationships were observed between measured spectra across all wavelengths (F_λ, 670–850 nm) and PAM fluorescence parameters under a range of actinic light intensities (steady-state fluorescence yields, F_t) and saturation pulses (maximal fluorescence yields, F_m). Our results suggest that this method can accurately reproduce the full Chl emission spectra – capturing the spectral dynamics associated with changes in the yields of fluorescence, photochemical (ΦPSII), and nonphotochemical quenching (NPQ).
- We discuss how this method may establish a link between photosynthetic capacity and the mechanistic drivers of wavelength-specific fluorescence emission during changes in environmental conditions (light, temperature, humidity). Our emphasis is on future research directions linking spectral fluorescence to photosynthesis, ΦPSII, and NPQ.

Introduction

The fate of photons absorbed by foliar pigments ultimately determines a leaf's capacity for photosynthesis. Upon being absorbed by a Chl molecule, a photon can follow three alternative pathways: photochemistry, heat loss (nonphotochemical quenching, NPQ), or Chl fluorescence (ChlF), all leading to the de-excitation of Chl (Kitajima & Butler, 1975; Genty *et al.*, 1989). During photosynthesis, the yields of photochemistry, NPQ, and ChlF are changed by feedback mechanisms that regulate the rate of electron transport (Govindjee, 1995), and the complex relationships among these three pathways makes predictions of one yield (i.e. photochemistry) from another (i.e. ChlF) challenging. Despite the close connection among ChlF, photosynthesis, and NPQ, their respective yields can only be unequivocally inferred when one or more of these three processes are inhibited. Pulse-amplitude modulation (PAM) fluorimetry is among the most widely used techniques to selectively open and close photosystem II (PSII) reaction centers to determine the photosynthetic quantum yields of absorbed photons (Krause & Weis, 1991; Bilger *et al.*, 1995).

Despite the popularity of PAM fluorimetry, the interpretation of such measurements is not straightforward (Logan *et al.*, 2007; Kalaji *et al.*, 2014). When the assumptions underlying PAM measurements are met, the technique can be applied widely at the leaf scale to track variation in the light reactions of photosynthesis (Maxwell & Johnson, 2000; Baker, 2008; Murchie & Lawson, 2013). PAM fluorescence is most often used to assess the efficiency of PSII photochemistry, which correlates strongly with CO_2 fixation (Genty *et al.*, 1989; Edwards & Baker, 1993).

However, this relationship breaks down in C_3 leaves when photorespiration occurs, the Mehler reaction is altered, or nitrate/sulfate is reduced (e.g. Fryer *et al.*, 1998; Logan *et al.*, 2007). The widespread use of PAM ChlF in photosynthesis research triggered interest in using remote sensing techniques to passively detect ChlF under solar illumination, so-called solar-induced Chl fluorescence (SIF; Meroni *et al.*, 2009; Porcar-Castell *et al.*, 2014 for reviews). In principle, SIF is proportional to the product of F_t (steady-state fluorescence yield, in PAM notations) and absorbed photosynthetically active radiation (aPAR), but an absolute calibration between the two metrics can be difficult as PAM measurements perform well for relative measurements but are not optimized for absolute radiometrically calibrated radiances. For example, deriving parameters related to electron transport (PSII efficiency) from PAM fluorescence requires a saturating light pulse (> 5000 μmol m^{-2} s^{-1}) to temporarily close PSII reaction centers, and a weak and pulsed modulating light beam (ML; Duysens, 1979) to track steady-state fluorescence yields. This method is not feasible from passive remote sensing platforms, limiting the information content of SIF in contrast to PAM measurements.

There are several challenges associated with the passive retrieval of ChlF compared with PAM. First, the SIF signal is small compared with the incoming solar irradiation and the reflectivity of terrestrial vegetation in the 650–850 nm range (1–5% of reflected light; see review by Meroni *et al.*, 2009). Second, because the ChlF emission spectrum overlaps with Chl*a*,*b* absorption spectra, up to 90% of red fluorescence photons can be reabsorbed by leaves (Gitelson *et al.*, 1998; Lichtenthaler *et al.*, 1998). Third, estimating wavelength-specific reabsorption and emission is complicated by the spectrum of the incoming light source, which often differs between the light-emitting diode (LED) source for PAM measurements and direct sunlight for SIF. The emission spectrum of the light source allows photons to penetrate into different leaf and canopy layers, resulting in wavelength-dependent scattering, absorption, and reabsorption throughout the canopy (Buschmann & Lichtenthaler, 1998; Vogelmann & Evans, 2002; Van Wittenberghe *et al.*, 2014, 2015). Moreover, the contribution of fluorescence differs between photosystems I (PSI) and PSII in that the contribution of PSI fluorescence is not affected by photochemical quenching as it lacks the back-transfer mechanisms of excitation into the antenna system (Franck *et al.*, 2002; Hasegawa *et al.*, 2010). PSI is also assumed not to be affected by NPQ, while PSII contributions to both red and far-red fluorescence are very dynamic (Genty *et al.*, 1990; Pfundel, 1998; Franck *et al.*, 2002). Lastly, changes in the ChlF emission spectrum during a saturation pulse, which drives the extrapolation of many PAM fluorescence parameters related to photosynthetic efficiency (quantum yield of photosystem II, ΦPSII) and stress (i.e. NPQ), are largely unknown (Franck *et al.*, 2002). Taken together, this makes validation of the SIF signal using PAM measurements challenging as a result of sampling inconsistencies in the spectral, temporal, and spatial domains.

Ground validation of remote sensing SIF signals often includes PAM measurements on individual plants taken within the sensor field-of-view (FOV), which are then averaged and extrapolated to the canopy scale (i.e. Louis *et al.*, 2005; Pérez-Priego *et al.*, 2005; Rascher *et al.*, 2009; Zarco-Tejada *et al.*, 2013). With increased mechanistic rigor, several pioneering studies have sought to connect PAM and spectral fluorescence in both time and space; for example, Moya *et al.* (2004) compared leaf-level active and passive fluorescence measurements (760 nm) during a dark–light transition and observed a strong linear relationship between the two ($R^2 = 0.99$). Amorós-López *et al.* (2008) demonstrated the ability of an instrument to simultaneously measure PAM and spectral ChlF (760 nm) over a diurnal cycle in an attempt to validate the Fraunhofer Line Discriminator principle (FLD, Plascyk & Gabriel, 1975) as a means of estimating fluorescence yield. Subsequently, Cendrero-Mateo *et al.* (2016) compared active and passive ChlF measurements at different temporal and spatial scales using a FluoWat leaf clip (Alonso *et al.*, 2007; Van Wittenberghe *et al.*, 2014), which is able to measure the whole ChlF emission spectrum using a short-pass filter (< 650 nm). They found that the relationships between passive and active ChlF were significant at the leaf scale but that complexities remained when results were extrapolated across an entire growing season and from leaf to canopy scales. Recently, Atherton *et al.* (2016) simultaneously measured ChlF using PAM and a spectrometer over a nearly identical leaf FOV and concluded that the wavelength-specific information of ChlF emission was an important factor for understanding the physiological mechanisms driving steady-state ChlF yield.

Despite the difficulties associated with the passive retrieval and interpretation of ChlF, substantial progress in the remote sensing of SIF has been made over recent decades at a range of scales (e.g. Gamon *et al.*, 1990; Zarco-Tejada *et al.*, 2003, 2012; Moya *et al.*, 2004; Meroni & Colombo, 2006; Guanter *et al.*, 2007; Damm *et al.*, 2010; Yang *et al.*, 2015). In these studies, remote sensing instruments that measure SIF have generally presented results from only one or a few wavelengths, as retrievals are often based on narrow atmospheric (O_2-A, O_2-B bands) or Fraunhofer lines (i.e. Meroni *et al.*, 2008; Cheng *et al.*, 2013; Yang *et al.*, 2015). Frequently, this has limited current studies to the *c.* 687 and 760 nm spectral ranges, which have been shown to provide important information on plant stress, though more research along these lines is needed (Ač *et al.*, 2015). A more complete understanding of the full ChlF emission spectrum across a range of vegetation conditions is particularly important given the recent interest in sampling the entire ChlF spectrum as proposed by the European Space Agency's fluorescence explorer (FLEX) mission concept (Drusch *et al.*, 2016). Part of the motivation behind the FLEX mission and the increasing interest in SIF is the rapidly increasing number of studies linking remotely sensed SIF from a single wavelength to gross primary photosynthesis (GPP) derived from eddy covariance flux towers (Walther *et al.*, 2015; Yang *et al.*, 2015; Wood *et al.*, 2016; Verma *et al.*, 2017). While these studies are promising, the direct link between spectral ChlF and concurrent measurements of CO_2 exchange at the leaf level has not been established. To obtain information more directly on plant–atmosphere CO_2 exchange, measurements of leaf-level gas exchange using infrared gas analyzers (IRGAs) have been widely used to infer rates and mechanics of photosynthesis (Long & Bernacchi, 2003). Unlike PAM fluorescence measurements, which

typically probe only a small leaf area (< 1 cm^2) in the top few layers of chlorenchyma, gas exchange techniques measure CO_2 flux over an integrated area across the thickness of a leaf. Together, gas-exchange measurements and PAM fluorescence can be used concurrently to investigate discrepancies between net CO_2 assimilation (A_{net}) and electron transport rates (ETRs) (e.g. Flexas *et al.*, 1999), mesophyll conductance rates (e.g. Flexas *et al.*, 2008), and variations in quantum yields of photochemistry, fluorescence, and heat dissipation.

Linking passively and actively induced ChlF and leaf-level gas exchange in both time and space could help to reveal the mechanisms underpinning the strong empirical association between remotely sensed SIF and GPP across a range of scales (i.e. satellite; Joiner *et al.*, 2011, 2013; Frankenberg *et al.*, 2011; Guanter *et al.*, 2012, 2014). For example, to better understand the relationships between SIF and GPP, including where the two processes converge and diverge, variations in NPQ must be taken into account. Through concurrent measurements of the yields of photochemistry (PAM), CO_2 exchange, and spectral ChlF radiances, we can explore the true information content that lies in the SIF signal. To accomplish this, we augmented a commercial gas-exchange and PAM instrument with a spectrometer system to measure absolute ChlF emissions across the entire 650–850 nm range. Here we place an emphasis on the methodology and suggest future research directions using results from a small dataset.

Materials and Methods

Instrument setup

The portable GFS-3000 gas-exchange and fluorescence system (Heinz Walz GmbH, Effeltrich, Germany) was slightly modified by using a spectrometer; a bundled fiberoptic (connecting the PAM fluorescence module and the spectrometer); an increased cuvette entrance hole to fit the wider bundled fiberoptic firmly into the leaf cuvette; and a short-pass filter below the incident light source (Fig. 1). These modifications, and the specifications of each instrument component are discussed later.

PAM fluorescence module

The manufacturer-provided fiberoptic PAM-Fluorimeter 3050-F was used to determine ChlF parameters (Heinz Walz GmbH; Fig. 1a). The PAM-Fluorimeter 3050-F includes a blue (LED) modulating light (ML) with peak emission of 450 nm (Supporting Information Fig. S1). The blue LED also drives the saturating pulse, which emitted a consistent 6000 µmol m^{-2} s^{-1} for 0.8 s for all measurements. The PAM-Fluorimeter 3050-F has only two modulation frequency settings (low, 10 Hz; high, 500 Hz). The modulation frequency was set to 'high' (500 Hz) in an attempt to capture the ML dynamics with the spectrometer

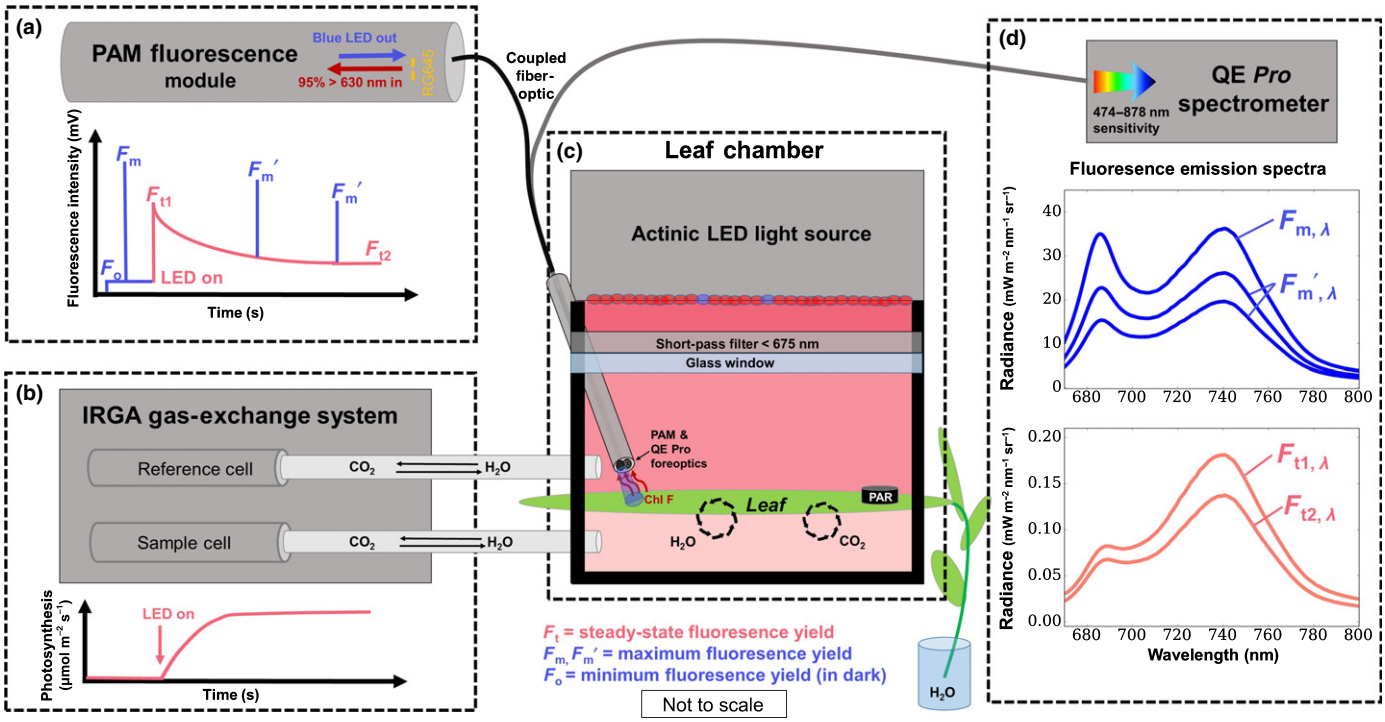

Fig. 1 Schematic of leaf-level measurement system. (a) Typical pulse-amplitude modulation (PAM) fluorescence trace during initial exposure to light. Note that the colors (blue and pink) represent the color of the light that is driving the signal even though all PAM parameters are computed from a blue light-emitting diode (LED). (b) Basic schematic of the infrared gas analyzer (IRGA) with a trace of a light response curve (showing net photosynthesis) under exposure to actinic light (similar in time to (a)). (c) Diagram of the leaf chamber, insertion of the fiberoptics from PAM and spectrometer (QE *Pro*), and the representative colors of light being emitted by the PAM and actinic LEDs. Note that the actinic LED light source is 90% red LEDs and 10% blue LEDs, and is somewhat attenuated by the short-pass filter (showing a slightly lighter 'pink' color beneath filter). A photosynthetically active radiation (PAR) sensor is placed at the leaf surface, and the coupled PAM and QE *Pro* foreoptic is *c*. 2 mm from the leaf surface. (d) Spectral fluorescence curves associated with $F_{m,\lambda}$ and $F_m'_{,\lambda}$ (driven by blue light) and $F_{t,\lambda}$ (driven by actinic LEDs) and corresponding times shown in the fluorescence trace in (a).

because when the ML light was set to 'low' (10 Hz) it was not possible to spectrally resolve the ML beam (see the Discussion section and the Supporting Information). The integration time for our spectrometer (minimum 8 ms) could not be matched with the modulation frequency of the LED, which did not allow us to measure the modulated emissions directly. However, by turning the ML beam on and off, we were able to detect the overall faint differences even at a 10 ms integration time (6 ± 1 binary units at 740 nm). The ML photosynthetically active radiation (PAR) at a 2 mm distance from the foreoptic to the leaf was 15 μmol m^{-2} s^{-1} under 'high-frequency' mode. The PAM-Fluorimeter uses a long-pass filter (RG645) with > 95% of the signal coming from beyond 645 nm (Fig. 1a). Before leaf insertion into the cuvette, a zero-offset was established using black nonfluorescing foam.

Gas-exchange system

The GFS-3000 uses two calibrated IRGAs to calculate a difference in CO_2 and H_2O concentrations in a reference and a sample cell during measurements (Long & Bernacchi, 2003; Fig. 1b). The IRGAs were used to compute net CO_2 assimilation (A_{net}), stomatal water vapor conductance ($g_{s(H2O)}$), transpiration rate (E), vapor pressure deficit (VPD), and intercellular CO_2 mole fraction (ci) over a 5 cm^2 rectangular leaf area (size of leaf adapter) according to manufacturer specifications (*GFS-3000 Handbook*, 7th edition © 2012; Heinz Walz GmbH). When ambient air was not used as the air flow intake, gas consisting of 2% O_2 and 98% N_2 was applied via a regulator and hose connected to the air intake for light response curves, and the flow rate was maintained at 750 μmol s^{-1} for all samples.

Light source and leaf chamber

The actinic light source was the manufacturer-provided LED 3040-L, which consists of a bank of 24 red and two blue LEDs (Figs 1c, S1; 90% red emission centered at 640 nm, and 10% blue emission with a peak wavelength of 470 nm; Heinz Walz GmbH). A homogeneous light distribution across the laminar leaf surface is assumed to be ± 20%. The actinic light source is capable of a range from 0 to 2000 μmol m^{-2} s^{-1} PAR. A small fraction of the light was attenuated by a short-pass filter which was affixed directly above the glass window on the leaf chamber to block incoming light transmission > *c.* 675 nm (Fig. 1c). The short-pass filter is a fused silica 50-mm-diameter filter with a 690–1000 nm rejection wavelength range, a > 91% 350–661 transmission wavelength range, and an optical density of 4 (Edmunds Optics, Barrington, NJ, USA; stock no: 84-726 (as of 29 August 2016)). PAR measurements at the leaf level were made directly above the leaf as shown in Fig. 1(c). Because no transmission data were collected, we were unable to compute the true aPAR and we assume an absorption coefficient k, where k is a commonly used leaf absorption coefficient, 0.84 (Baker, 2008; Tubuxin *et al.*, 2015).

The 1.5-mm-diameter fiberoptic cable from the PAM fluorimeter was affixed to three 200 μm fibers (one fiberoptic cable) connected to the spectrometer and was sealed with a black rubber coating to prevent light transmission along the optical path. The bundled foreoptic (Fig. 1c) was in a steel housing which was inserted firmly into the leaf chamber (to prevent air leakage from the chamber) at an angle of *c.* 60° and a distance of *c.* 2 mm to the leaf to approximate nadir without shading the FOV, and ensure complete light saturation from pulses.

Spectrometer

Spectral radiant energy fluxes were measured using a QE *Pro* high sensitivity spectrometer (Ocean Optics, Dunedin, FL, USA; Fig. 1d). The detector covers 474–858 nm at 3 nm spectral resolution with a spectral sampling of 0.35 nm. Absolute calibration of the QE *Pro* spectrometer was done using an integrating sphere and a reference ASD spectrometer (Analytical Spectral Devices Inc., Boulder, CO, USA) at the Jet Propulsion Laboratory in Pasadena, California. In addition, we verified that detector nonlinearity across the signal intensities we typically observe was < 1% and could thus be ignored in our study. Therefore, a linear calibration factor after subtraction of the dark current readout was used. Spectra were measured at an interval of 10 ms (integration time) and 20 spectra were co-added, resulting in a stored data record every 0.2 s. These integration and averaging times were chosen to avoid optical sensor saturation at the highest light intensities and to provide an unbiased data point during the middle of the saturation pulse (0.8 s).

Experiment design

Four light response curves were generated for two leaves (one from *Acer palmatum* Thunb. and one from *Quercus lobata* Née). Mature leaves were collected from the south-facing side of irrigated trees on the California Institute of Technology campus (Pasadena, CA, USA). Terminal branches of five to six leaves were clipped with shears and the stem of the branch was immediately placed and recut under water before being moved to a completely dark room for > 2 h to facilitate dark adaptation. For both species, a mature terminal leaf attached to the stem was used to generate a light response curve in 'nonstressed' conditions (controlled cuvette conditions, leaf temperature at 25°C; relative humidity (RH) at 60%: Table 1). Aside from modifications made to the leaf chamber environmental conditions, consistent alternating current (AC) power to the instruments and room temperature (24°C) were maintained for the duration of the experiment.

The light response curves and subsequent time for each light regime of *Q. lobata* were as follows (in μmol m^{-2} s^{-1} PAR): 50 (9.5 min), 100 (9.5 min), 200 (9.5 min), 400 (10.5 min), 600 (11.5 min), 900 (11.5 min), 1200 (11.5 min), 1500 (11.5 min). For *A. palmatum*, each light regime was shortened by 2 min (light response curves are shown in Fig. S2). Following generation of the initial light-response curve in 'nonstressed' conditions, the leaf was kept in the cuvette (to ensure the same spectrometer and PAM FOV), the LED light source was turned off, and temperature was increased to 40°C and H_2O concentration reduced to 13% RH within the chamber (Table 1). Following another > 2 h dark-adaptation period, an identical light-response curve was

Table 1 Summary of sampling conditions during each light response curve

Species	Condition	T (°C)	RH (%)	CO_2 (ppm)	H_2O (ppm)	O_2 (%)	ML test?
Acer palmatum	Nonstressed	25 ± 0.02	60 ± 1%	380	20 000	21.0	No
A. palmatum	Stressed	40 ± 0.02	13 ± 1%	380	10 000	21.0	No
Quercus lobata	Nonstressed	25 ± 0.02	60 ± 1%	380	20 000	2.0	Yes
Q. lobata	Stressed	40 ± 0.02	13 ± 1%	380	10 000	2.0	Yes

ML, a protocol involving turning the modulating light beam off for 30 s during each light regime; T, temperature; RH, relative humidity inside the cuvette, with ± 1 SE around the mean.

generated under the 'stressed' condition. Throughout the course of each light response curve, PAM F_t and gas-exchange data were collected in synchrony every 5 s, and saturation pulses (F_m) were recorded every 30 s (Atherton *et al.*, 2016). The clock from the PAM/gas-exchange instrument and QE *Pro* were synced for ease of data analysis. A complete time series of the PAM and spectral fluorescence for both species and conditions are shown in Fig. S3. This experimental procedure was similar for both *A. palmatum* and *Q. lobata* except for two differences: the *Q. lobata* samples were run under low O_2 (2% O_2 and 98% N_2) air conditions inside the cuvette to inhibit photorespiration and improve the interpretation of quantum yields; and we included an ML beam test (hereafter, 'ML-on-off test') to directly compare fluorescence parameters derived from the ML beam alone (as with traditional PAM F_t measurements, shown in the Figs S4, S5).

Analysis of PAM and fluorescence spectra

It is important to note the fundamental differences between F_λ from the spectrometer and F_t from PAM. F_λ is the absolute radiant energy flux of ChlF as derived from remote sensing platforms (Eqn 1):

$$F_\lambda = \text{aPAR} \times \Phi F \times \varepsilon_\lambda \quad \text{Eqn 1}$$

where ΦF is the probability an absorbed photon will be fluoresced and escape the leaf/canopy, and ε_λ is the probability a fluoresced photon will have wavelength lambda. Because every F_λ retrieval is not from direct sunlight in this study (i.e. SIF), but a combination of blue (10%) and red (90%) LEDs, we use F_λ notation to describe all spectrally resolved fluorescence retrievals. By contrast, F_t from PAM can be expressed as:

$$F_t = \text{aPAR}_{ML} \times \Phi F \times \varepsilon_P \quad \text{Eqn 2}$$

where aPAR_{ML} is the absorbed radiant energy from the blue modulating light, and ε_P is the integral of ε_λ from the PAM long-pass filter (95% > 645 nm). Eqns 1 and 2 are simplified models as both ε and ΦF are dependent on the spectral shape of both the illumination source and photochemical status of the plant (for more detailed models see Porcar-Castell *et al.*, 2014, e.g. Eqn 20).

There are several key differences between PAM fluorescence parameters and the spectrally resolved data. Apart from F_t being analogous to a numerical derivative of spectrally integrated F_λ with respect to changes in aPAR, it should be noted that both are driven by different light sources in our setup, which requires future changes to enable a more direct comparison. All PAM measurements are derived solely from blue LED emission, for both the ML beam (F_t) and the saturation pulses (F_m, Fig. S1), whereas, in the case of $F_{m,\lambda}$, the measured fluorescence spectra are driven primarily by blue light, but with an added *c.* 0–25% influence from the actinic light, depending on actinic light intensity. F_λ, on the other hand, is driven by the actinic light source LEDs only. An additional consideration is that spectral data are integrated every 10 ms but coadded over a much shorter time span (0.2 s) than the ML beam, which produces a data record every 2 ms at 500 Hz and is averaged over 5 s intervals. With a 10 ms integration time for the QE *Pro* and a 500 Hz PAM frequency, five pulses of measuring light are enough to separate the spectra induced by the ML beam and the actinic light (Figs S4, S5). Ideally, full control of the ML beam frequency allows synchronization between the two instruments.

Fig. 2 conceptually diagrams the beginning of each light response curve, and resulting data from the QE *Pro* (F_λ) and PAM fluorimeter (F_m, F_m', F_t).

At the beginning of each light response curve, the ML was turned on to derive a minimal ChlF yield (F_o, in Fig. 2b,c, when photosystem reaction centers are assumed to be completely open). After 15 s of 'ML-on', the first saturation pulse was applied and F_m from the PAM and spectra ($F_{m,\lambda}$) were derived (Fig. 2a). During this initial pulse of light (F_m), it is assumed that reaction centers are effectively closed, thus enabling inference of maximal ΦPSII. Fifteen seconds following the initial saturation pulse, the actinic light was turned on to 50 μmol m^{-2} s^{-1} PAR (Fig. 2b,c). Following 15 s of actinic light exposure, subsequent saturation pulses were applied every 30 s throughout the light response curve to determine maximum Chl*a* fluorescence yield in the light-adapted state (F_m' and $F_{m,\lambda}'$) (Fig. 2a). Upon each transition to increased light, a reduced immediate fluorescence quenching efficiency could be observed – the 'Kautsky' effect (Fig. 2b; Kautsky & Hirsch, 1931).

Every data record from the spectrometer is output and averaged or indexed during analysis. To compare data between PAM/gas-exchange and spectra, F_λ was averaged over the identical 5 s PAM/gas-exchange data record. To compare F_m values between PAM and spectra, we subtracted F_λ immediately before the

New Phytologist

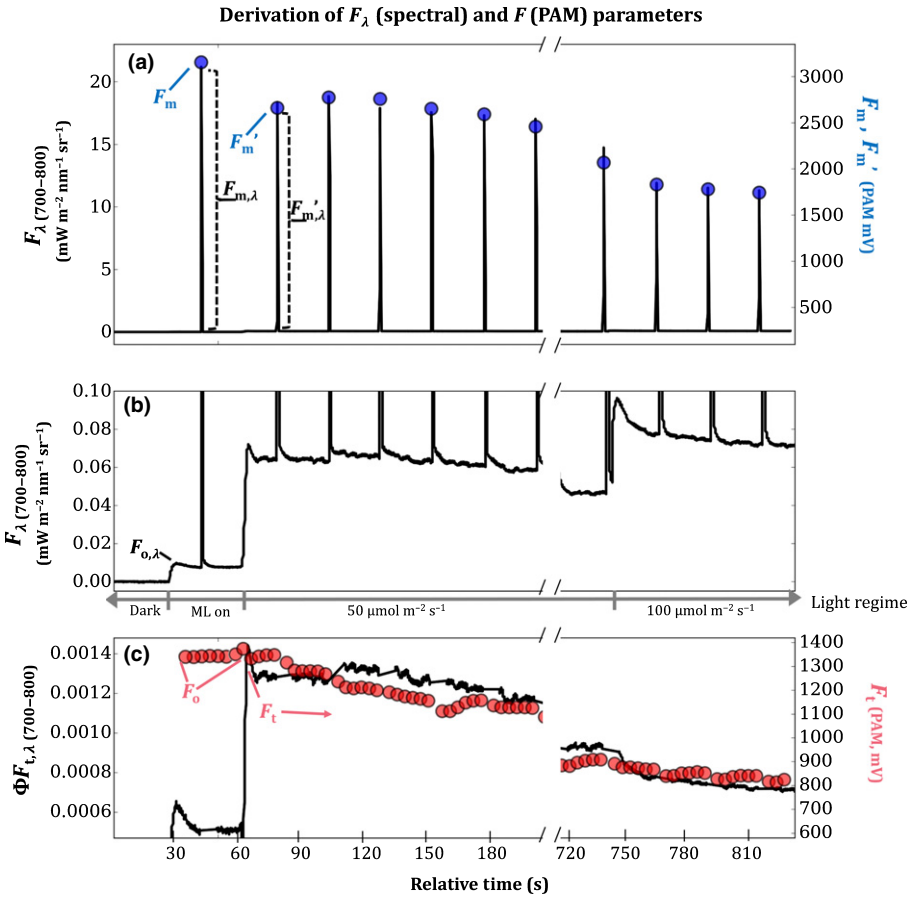

Fig. 2 Conceptual figure highlighting the derivation of spectral fluorescence (F_λ) and fluorescence parameters from pulse-amplitude modulation (PAM) during the beginning of the light response curve (including the first and second light regimes). (a) Derivation of maximal fluorescence parameters from spectra ($F_{m,\lambda}$, $F_m'_{,\lambda}$) and PAM (F_m, F_m'); (b) an enlarged version of (a) (note *y*-axis units) highlighting the spectral fluorescence signal (F_λ), analogous to solar-induced fluorescence (SIF); (c) fluorescence intensity derived from PAM (F_t), which is not sensitive to absorbed light (aPAR), overlain with spectral fluorescence yield ($\Phi F_{t,\lambda} = F_\lambda$/aPAR × leaf absorption). This example is from the *Quercus lobata* run under nonstressed conditions, and the spectra are an average of the 700–800 nm range. For a more detailed and exhaustive description of parameters, see Supporting Information Fig. S6.

maximal $F_{m,\lambda}$ value during the saturation pulse. As the saturation pulse always has the same intensity, and as we subtract F_λ from $F_{m,\lambda}$ immediately before the pulse, the result is independent of light, similar to an F_m yield measurement from PAM. Note that yield computation for $F_{m,\lambda}$ is confounded by differing emission light sources between the red actinic light and blue saturation pulse. The ChlF yield ($\Phi F_{t,\lambda}$), as shown in Fig. 2(c), is the ratio of fluoresced photons to absorbed photons and is computed according to Table 2 by dividing F_λ by PAR at the leaf level × k (absorption coefficient), following the conversion of PAR from µmol m^{-2} s^{-1} to mW m^{-2} s^{-1}. Computing spectral fluorescence yields, $F_{m,\lambda}$ and $\Phi F_{t,\lambda}$, allows for a more direct comparison with PAM F_m and F_t parameters by accounting for incoming radiant energy fluxes – with some caveats discussed later. ΦCO_2 was calculated by dividing A_{net} (µmol m^{-2} s^{-1}) by leaf PAR (µmol m^{-2} s^{-1}) × k. All PAM fluorescence parameters (ΦPSII, NPQ) were computed according to traditional nomenclature and are provided in Table 2. Additional parameter computations and data from these parameters are shown in the Supporting Information (Table S1; Fig. S6).

SCOPE simulations

As a means for comparison, and to demonstrate the potential for using datasets derived using this method in a radiative transfer modeling framework, we also looked at the relationship between ΦF_t and ΦPSII within the Soil Canopy Observation of Photosynthesis and Energy (SCOPE) model (v.1.61, van der Tol *et al.*, 2014). The SCOPE model simulates leaf and canopy fluorescence, photochemistry, and NPQ, with the sum of the three alternative pathways always equal to 1. In this model, the photosynthesis yield is first computed based on the Farquhar model (Farquhar *et al.*, 1980), then a fluorescence yield is derived based on a parameterization of ΦF_t vs ΦPSII derived from leaf-level PAM fluorescence measurements under different conditions. The model provides two different parameterizations to approximate the likely range that plants will experience in the field (here referred to as SCOPE 1 and SCOPE 2), both of which were used to compare the variation in ΦF_t and ΦPSII with our own data. In this simple example, the default parameters provided in SCOPE v.1.61 were used.

Table 2 Nomenclature for parameters derived from pulse-amplitude modulation (PAM) fluorescence and spectrally derived fluorescence (F_λ)

PAM parameter	PAM units	PAM calculation	PAM measuring interval	PAM measuring frequency	Light source driving F_{PAM} parameter	Spectral parameter	Spectral units	Spectral parameter calculation	Spectral measuring interval	Light source driving F_λ parameter	Traditionally known as
F_m F_m'	mV	DC voltage above baseline ($\int$mV > 700 nm)	0.8 s sat. width	Once post-dark adaptation; and then every 30 s	Blue saturation pulse	$F_{m,\lambda}$ $F_m'_\lambda$	mW m^{-2} nm^{-1} sr^{-1}	Maximum F_λ recorded during saturation pulse $- F_\lambda$ immediately before each pulse.	0.2 s avg.; 10 ms int.	Blue saturation pulse + actinic light	Maximum Chl*a* fluorescence radiant flux in dark-adapted state (F_m) and in light-adapted state (F_m')
na	na	na	na	na	na	F_λ	mW m^{-2} nm^{-1} sr^{-1}	F_λ	0.2 s avg.; 10 ms int.	Blue modulated light + actinic light	Solar-induced Chl fluorescence (SIF). In this case, red and blue LEDs.
F_t	mV	DC voltage above baseline ($\int$mV > 700 nm)	5.0 s avg.; 1.0 s int.	Every 5 s	Blue modulated measuring light	$\Phi F_{t,\lambda}$	(mW m^{-2} nm^{-1})/ (mW m^{-2})	$(F_\lambda)/(k * PAR)$	0.2 s avg.; 10 ms int.	Blue modulated light + actinic light	Fluorescence yield: PAM and spectra analogous but not identical measurements
ΦPSII	0–1.0, relative yield	$(F_m' - F_t)/(F_m')$	F_t immediately before F_m'	Every 30 s	Blue saturation pulse and modulated measuring light	na	na	na	na	na	Photosystem II yield; photosynthetic efficiency
NPQ	> 0	$(F_m - F_m')/(F_m)$	0.8 s sat. width	Every 30 s in the light	Blue saturation pulse and modulated measuring light	na	na	na	na	na	Nonphotochemical quenching of Chl fluorescence

Derivation of parameters, such as absolute units, their calculation, measuring interval (including averaging period (avg.) and integration time (int.), and frequency are provided). F_m, maximal fluorescence yield from PAM; $F_{m,\lambda}$, maximal fluorescence from spectra; F_t, transient fluorescence; $\Phi F_{t,\lambda}$, spectral fluorescence yield; ΦPSII, photosystem II yield; NPQ, nonphotochemical quenching; LED, light-emitting diode; PAR, photosynthetically active radiation; DC, direct current. Note that the rows where 'na' is present represent spectral or PAM parameters that cannot be directly compared with each other. Rather, PAM parameters can be estimated by spectral parameters by multiplying the probability that an absorbed photon will be fluoresced at a given wavelength range $\Phi F_{t,\lambda}$ by the probability that a fluoresced photon will have wavelength × (ε_λ) and absorbed light (aPAR), as seen in Eqn 1. An absorption coefficient (k) of 0.84 is assumed in the computation of spectral fluorescence yields.

Results

Relationships between F_λ (spectral) and F (PAM) parameters

An example of the relationships among PAM yields and spectral fluorescence yield parameters is provided from *Q. lobata* (nonstressed) in Fig. 3(a,c) and a summary of the wavelength-specific relationships for both species and conditions is shown in Fig. 3(b, d).

Strong linear relationships were observed between all dark- and light-adapted maximal fluorescence yield parameters ($F_{m,\lambda}$, $F_m'_{,\lambda}$ and F_m, F_m') across all wavelengths for each species and condition ($0.89 > R^2 > 1.00$; Fig. 3b). The wavelength -specific R^2 between $\Phi F_{t,\lambda}$ and PAM F_t intensity ranged from 0.73 to 0.95, with consistency in coefficients of determination across all wavelengths, and small decreases at the far ends of the F emission spectrum (Fig. 3d); however, the slope varied, since it is fully determined by the average spectral shape of the fluorescence emission (according to Eqn 1).

Chlorophyll fluorescence emission spectra, $F_{m,\lambda}$ and F_λ, for both species and conditions during the entire light response curve are shown in Fig. 4.

The absolute magnitude of spectra were considerably higher under nonstressed than stressed conditions for $F_{m,\lambda}$, $F_m'_{,\lambda}$ and F_λ (Fig. 4). Changes in the magnitude of F_λ throughout each experiment are largely driven by PAR, while the differences in $F_m'_{,\lambda}$ spectra are driven by gradual changes in fluorescence quenching efficiency over time. $F_m'_{,\lambda}$ behaves like a fluorescence yield because the saturating pulse is always the same intensity and is subtracted by F_λ measured before the $F_{m,\lambda}$ measurement.

The relative differences in fluorescence emission under differing light sources, species, stress levels, and over time are shown in Fig. 5.

There are substantial differences between the first ChlF emission peak when observed under blue (Fig. 5a) and red (Fig. 5b) light sources. At increased light intensities, there is a drop in both $F_m'_{,\lambda}$ (Fig. 5a) and F_λ (Fig. 5b) in the first emission peak, while the second emission peak remains relatively unchanged; however, the first emission peak is exaggerated as we normalized the data by the maxima near 740 nm. It is also worth noting that the blue and red light were not compared under fair conditions – one is saturating and the other is actinic (see the Discussion section).

As an example of how this work could be used in future applications, we plotted the relative changes in F_t from PAM and $\Phi F_{t,\lambda}$ against NPQ, ΦPSII, and ΦCO_2 from *A. palmatum* (nonstressed) (Fig. 6).

All example wavelengths changed in a similar fashion to PAM F_t when compared against NPQ (Fig. 6a), ΦPSII (Fig. 6b), and ΦCO_2 (Fig. 6c). However, relative differences were observed in

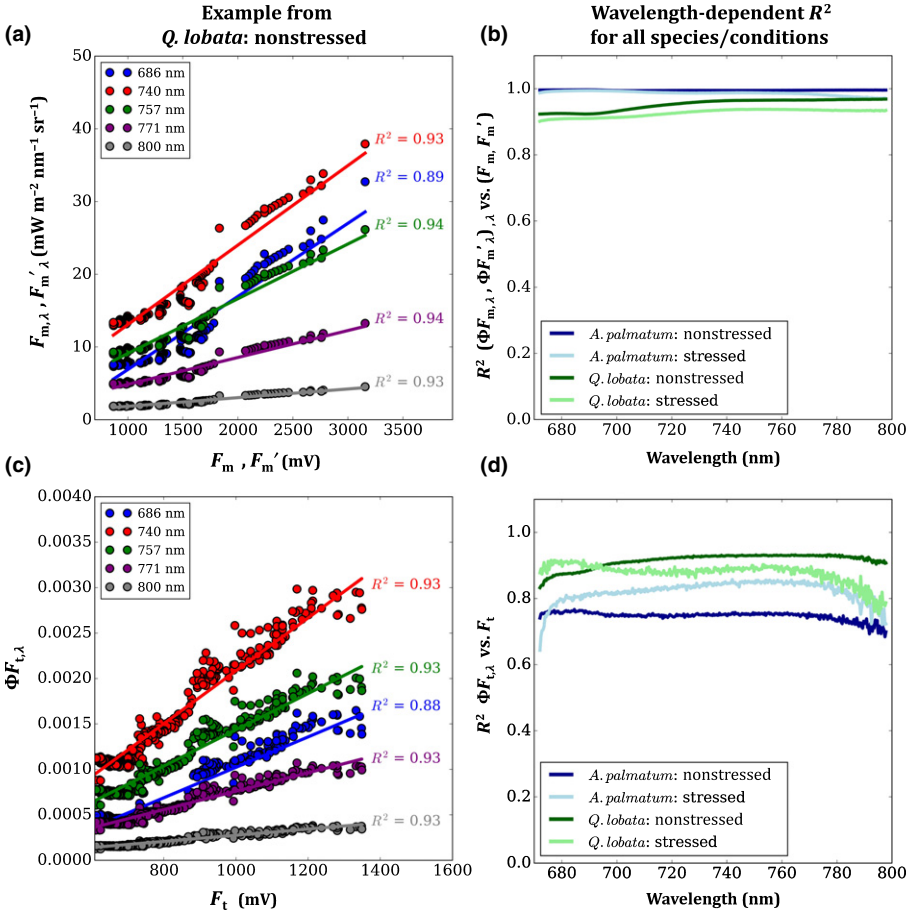

Fig. 3 (a) Relationship between maximal fluorescence yield (F_m and F_m') derived from pulse-amplitude modulation (PAM) and from spectra ($F_{m,\lambda}$ and $F_m'_{,\lambda}$) with five example wavelengths (686, 740, 757, 771, and 800 nm) taken from *Quercus lobata* (nonstressed). (b) Coefficient of determination (R^2) for each wavelength of maximal fluorescence yield relationships for both species and conditions. (c) Relationship between transient fluorescence (F_t) derived from PAM and spectral fluorescence yield ($\Phi F_{t,\lambda}$). (d) Coefficient of determination (R^2) for each wavelength of steady-state fluorescence yields relationships for both species and conditions.

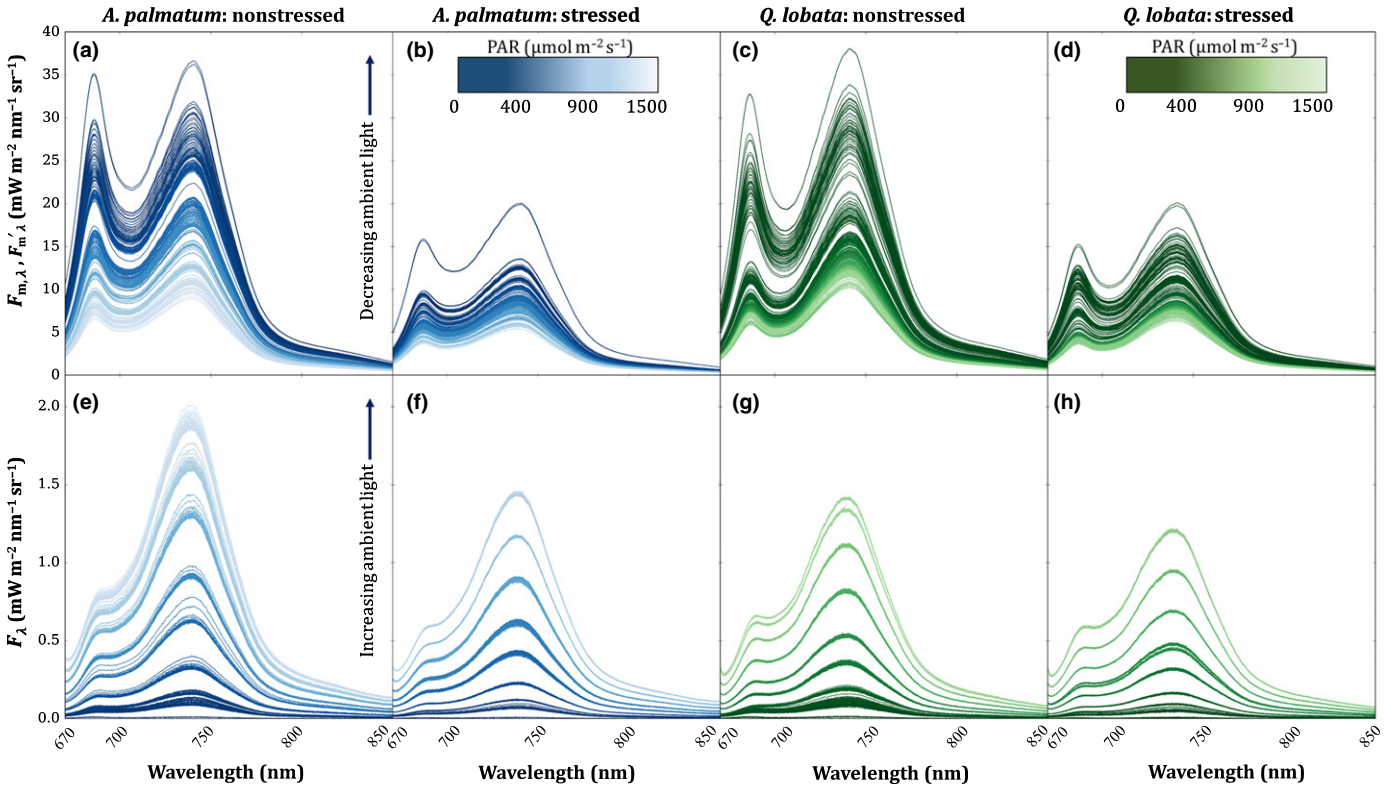

Fig. 4 Maximal fluorescence emission derived from the saturation pulse ($F_{m,\lambda}$ and $F_{m',\lambda}$) (a–d) and actinic light-induced fluorescence emission (F_λ) (e–h) among *Acer palmatum* (blues) leaves under nonstressed (a, e) and stressed (b, f) conditions; and *Quercus lobata* (greens) leaves under nonstressed (c, g) and stressed (d, h) conditions. Color ramp is indicative of incident photosynthetically active radiation (PAR, μmol m^{-2} s^{-1}) exposure during light response curve – lighter colors indicate greater PAR, and darker colors represent less incident PAR.

$\Phi F_{t,\lambda}$ on the order of 10–30% depending on the emission wavelength observed. We overlaid two versions of the ΦPSII vs ΦF_t relationship as would be expected from the SCOPE model to show how our data might be used to inform such relationships in a modeling framework.

Empirically derived leaf-level relationships between net photosynthesis (A_{net}) and steady-state fluorescence radiant energy flux (as would be observed from remote sensing platforms) are provided in Fig. 7.

The relationships among $F_{\lambda,686}$, $F_{\lambda,740}$ and A_{net} show nonlinear, wavelength, species, and condition-dependent responses to light environment (Fig. 7). For both F_{686} and F_{740}, the stressed treatments show continually increasing F_λ after photosynthesis was light-saturated, but at a smaller magnitude than the nonstressed treatments.

Discussion

We modified an existing leaf-level gas-exchange/fluorescence instrument to simultaneously measure PAM fluorescence, spectral radiant fluorescence (F_λ), and CO_2 fluxes. Such coincident measurements will help to provide the basis for subsequent studies assessing the impact of changes in the spectral shape of ChlF emission accompanying traditional PAM and photosynthesis measurements. Here we touch on the implications of our findings but place greater emphasis on how our methodology can be improved upon and used in the future with examples from this dataset.

The instrument described here successfully captured the spectral dynamics of steady-state and maximal fluorescence under a range of light conditions (Figs 3–5). Results from this study suggest that while the relationship between spectral ChlF yields and PAM F yields is consistently strong, it is also wavelength-dependent, with the slope following the average shape of the fluorescence emission curve (see Eqn 1). The strength of this relationship is not surprising, considering that PAM fluorescence is derived from a broadband signal; moreover, it is an important consideration for scaling exercises comparing leaf-level based PAM measurements to canopy-level SIF (e.g. Zarco-Tejada *et al.*, 2013). Deriving an F_λ value can allow for direct comparisons in absolute radiant energy flux units across species and conditions, by contrast to differences in the magnitude of a unitless (relative) PAM measurement. A desirable future development in the computation of absolute $\Phi F_{t,\lambda}$ and $F_{m,\lambda}$ would be an accurate estimate of aPAR, instead of one based on an approximation of the absorption coefficient, *k*. To accomplish this, one could place a PAR sensor below the leaf to compute leaf transmission in conjunction with leaf reflectance measurements. Leaf reflectance data could be computed through normalization with a pure reflectance spectra from a white Lambertian diffuser plate (i.e. Spectralon) placed under the foreoptics during a light response curve (as in Magney *et al.*, 2014).

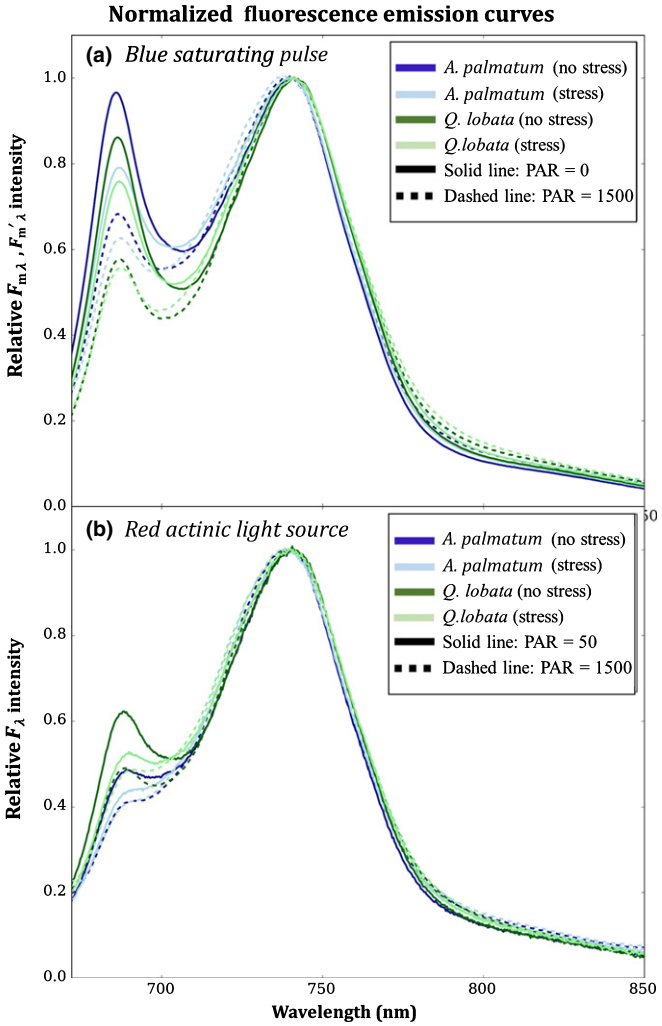

Fig. 5 (a) Relative differences in maximum spectral fluorescence emission ($F_{m,\lambda}$ and $F_{m',\lambda}$) curves for both species and conditions, normalized to a maximal $F_{m,\lambda}$ or $F_{m',\lambda}$ radiance value at each time period when photosynthetically active radiation (PAR) = 0 (solid lines) and PAR = 1500 (dashed lines). (b) Relative differences in steady-state spectral fluorescence (F_λ) emission curves for both species and conditions, normalized to maximal F_λ radiance value at each time period during PAR = 50 (solid lines) and PAR = 1500 (dashed lines). Note that most of the emission light source is coming from the blue light-emitting diode (LED) in (a) and red in (b).

Our results further suggest the importance of quantifying both NPQ and ΦPSII, both of which can alter the yields of Chl fluorescence in different, nonlinear ways (Fig. 6). This example shows that increased NPQ and decreased ΦPSII generally reduce the normalized ChlF yield across the entire spectral range at a similar magnitude to changes in F_t from PAM, which represents an integrated signal from > 645 nm driven by blue light, thus only penetrating the upper leaf layers (Agati, 1998; Buschmann, 2007). In this example, under low light conditions, we see a rapid change in $\Phi F_{t,\lambda}$ and F_t before substantial changes in NPQ, indicating that under low light, changes in the quantum yield of photochemistry and fluorescence are primarily controlled by photochemical quenching (PQ), whereas at higher light, changes in ChlF and ΦPSII are primarily driven by NPQ (Porcar-Castell *et al.*, 2014). The inverted 'V' relationship between ΦPSII and $\Phi F_{t,\lambda}/F_t$ is shown in Fig. 6(b), although not to the same extent as that observed in Flexas *et al.* (2002) (SCOPE 1) or van der Tol *et al.* (2014) (SCOPE 2), which is probably explained by the lack of data representing higher and lower ΦPSII from this example. The two SCOPE parameterizations are based on limited datasets of grapevine plants exposed to drought stress (SCOPE 1) and cotton leaves under a range of temperature conditions (SCOPE 2). The different behaviors of these curves underscore the need for increased datasets – with wavelength dependencies – across a range of species and conditions to drive such models. In addition, samples with different photosynthetic capacities should be measured under a wider range of light, temperature, humidity and CO_2 conditions to further investigate the spectrally dependent nonlinearities amongst ChlF, NPQ, and ΦPSII, and how they might vary with actual ΦCO_2. In the example shown in Fig. 6(c), we observed a saturation and subsequent decrease of ΦCO_2 at *c.* 600 μmol m^{-2} s^{-1} PAR, while ChlF yield continued to decrease as light intensity increased. Datasets such as this could be important considering modeled CO_2 yields vary with light, atmospheric CO_2, and humidity as typically predicted with the Farquhar–von Caemmerer-Berry model (Farquhar *et al.*, 1980); whereas ChlF yields respond to environmental conditions that affect PQ and NPQ (Porcar-Castell *et al.*, 2014). Beyond this example, with a robust number of samples covering a wide range of conditions, one could compute the full ChlF excitation emission matrix (EMM) to drive radiative transfer models (i.e. van der Tol *et al.*, 2009, 2014; Vilfan *et al.*, 2016). When computing the EMM it is important to consider the spectral shape of the illumination source and the actual number of photons absorbed by the chloroplast (aPAR). Additionally, interpretation of the results could be further improved by including data on plant pigments, where we could observe changes in xanthophyll cycle pigment concentrations under illumination (similar to Magney *et al.*, 2017), permitting better characterization of the interactions among leaf pigment concentrations (particularly Chl) and leaf morphology to better understand the biophysical contributions of fluoresced photons.

Another advantage of this method is the high spectral sampling frequency (such as 0.2 s shown here) to observe the fast-response kinetics of ChlF quenching (Franck *et al.*, 2005; Buschmann, 2007). In our case, we observed a substantial 'Kautsky effect' from the *A. palmatum* samples (Figs 2, S3), which could be attributed to slower reoxidation of plastoquinones in PSI and NPQ at a much greater magnitude than in the low-O_2 treatments involving *Q. lobata* (Brody & Rabinowitch, 1957). From our limited dataset, we found that the shape of the fluorescence emission curve > 720 nm was relatively stable regardless of illumination over time (Figs 4, 5, S7); however, there were substantial differences in the fluorescence spectrum in the first emission peak (670–720 nm) with increasing PAR (Figs 5, S7). Changes in the shape of the ChlF spectrum shown here could have multiple explanations, including changes in Chl reabsorption or NPQ components during illumination (Lambrev *et al.*, 2010). The development of a method to measure the complete ChlF emission spectrum at high temporal frequencies will enable future

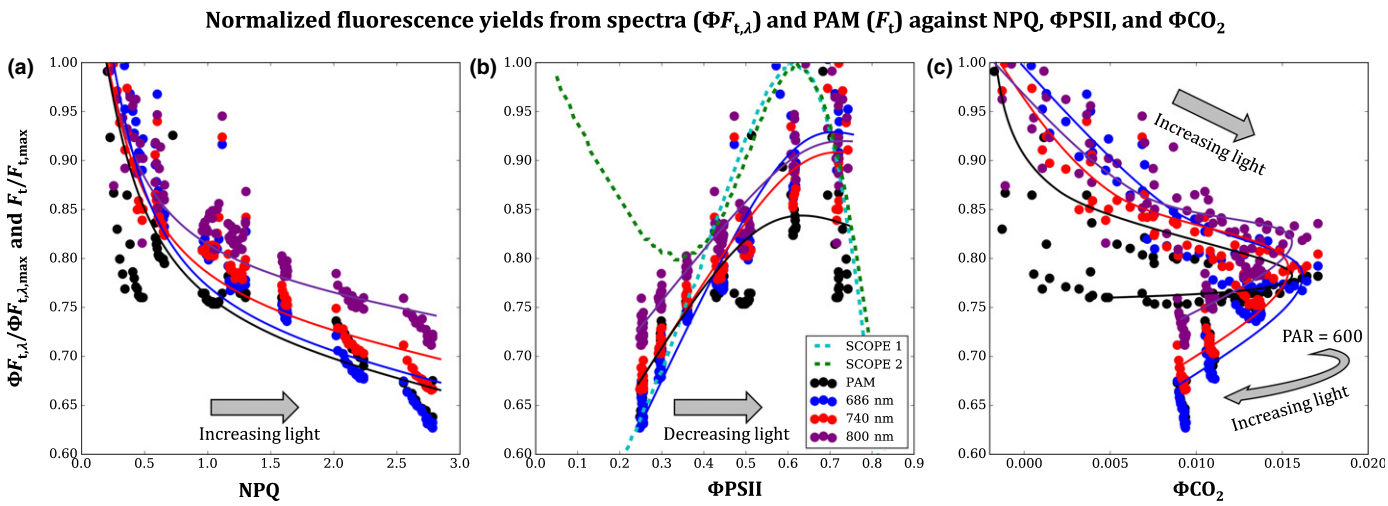

Fig. 6 Relative changes in steady-state fluorescence yields from pulse-amplitude modulation (PAM) (F_t) and spectra ($\Phi F_{t,\lambda}$: wavelengths 686, 740, 800) against nonphotochemical quenching (NPQ) (a), photosystem II yield (ΦPSII) (b), and CO_2 yield (ΦCO_2) (c) for *Acer palmatum* (nonstressed) during the course of the light response curve. In (b), results are overlain with modeling results from the Soil Canopy Observation of Photosynthesis and Energy (SCOPE) model using two parameterizations (see the Materials and Methods section; they are called SCOPE 1 and SCOPE 2 here). The PAM and spectral Chl fluorescence yield data are normalized to the maximum during the light response curve. Polynomial models were fitted to all relationships for trend visualization purposes.

investigations into wavelength dependencies associated with the suppression of the primary electron acceptor (quinone A) during PQ by PSII, for example. (Franck *et al.*, 2002, 2005; Pedrós *et al.*, 2008).

The emission peak of the illumination source is another key consideration for future studies, particularly among the ML, saturating pulse, and actinic light sources. From Fig. 5, one can deduce that the first emission peak centered at 686 nm appears somewhat more affected but the interpretation of changes in the two fluorescence peaks is complicated by the possibility of light reabsorption within the leaf (Buschmann & Lichtenthaler, 1998; Gitelson *et al.*, 1998). Under white light LEDs or natural sunlight, for example, the fluorescence signal comes from both surface and deeper leaf layers (Vogelmann, 1993; Rappaport *et al.*, 2007) and is thus more likely to be reabsorbed, whereas the blue LED used here primarily affects the upper leaf surface, resulting in a shorter path to escape the leaf without being reabsorbed (Agati, 1998; Vogelmann & Evans, 2002). To complicate matters, there can be gradients of NPQ within a leaf, which might change the distribution of photochemical and fluorescence quenching with leaf depth and thus affect the first fluorescence peak through changes in red ChlF reabsorption (Anderson *et al.*, 1988). Future measurements using different peak emission λ LEDs (i.e. white) and measurements of F_λ under natural sunlight are needed and are feasible using a short-pass filter at 675 nm similar to the one described here, provided that incident light is perpendicular to the filter.

Using a white LED approximating solar irradiance for all incoming light sources will require full control over the modulation frequency to optimize integration time and spectral detector

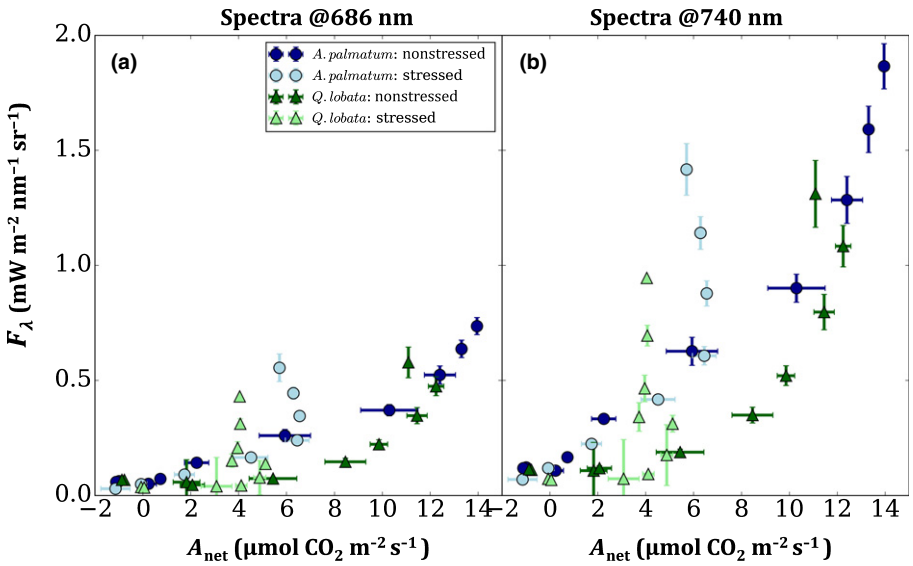

Fig. 7 (a, b) Relationships among steady-state spectral fluorescence (F_λ) and photosynthesis (A_{net}) for wavelengths of 686 nm (a) and 740 nm (b) for both species and conditions. Points are the means of steady-state A_{net} and F_λ during each light regime and error bars represent ± SE experienced during each light regime.

sensitivity, and promote temporal synchronization between the spectrometer and ML. To test the ability of the QE *Pro* to capture the ML signal, we developed a technique (ML-on-off) to derive an $F_{ML,\lambda}$ solely from the ML beam. This permitted the comparison of ΔF_λ from ML-on and ML-off with F_t from PAM, and showed a strong correlation ($R^2 > 0.91$ for all wavelengths; Figs S4, S5). In this study, a relatively high modulating frequency was used for the ML beam (500 Hz) in order to extract a spectral radiance signal, which may create an actinic effect on the leaf despite higher signal-to-noise ratio (Schansker *et al.*, 2006). Ideally, we would synchronize the ML beam with the QE *Pro* readout to measure the full spectrum induced only by the ML beam. This was beyond the scope of the current study but could be achieved with lower-frequency ML (< 50 Hz) and readout rates as low as 8 ms from the spectrometer. Nonetheless, the results shown in Figs S4 and S5 are promising considering the extremely small contribution of the ML to total actinic light (1.5% at the highest and 30% at the lowest light intensities).

Connecting remote sensing measurements of F_λ with gross photosynthesis

At the leaf scale, we demonstrate simple environmentally and species-different relationships between F_λ and A_{net} (Fig. 7) for each light response curve in the experiment. In the example shown in Fig. 7, a nonlinear relationship between F_λ and A_{net} was observed for both species and conditions, whereby F_λ continued to increase after A_{net} reached light saturation (Fig. 7). As has been shown in previous studies (i.e. Flexas *et al.*, 2002), the absolute magnitude of F_λ is reduced under stressed conditions, but to a lesser degree than A_{net}, which approached light saturation at increasing light intensities (Figs 7, S2). The nonlinear relationships between F_λ and net photosynthesis observed at the leaf scale are to be expected when the capacity for photosynthesis is reached, as the light-dependent reactions associated with photosynthesis produce more ATP and NADPH than can be used by the light-independent reactions for CO_2 fixation; meanwhile, an increased number of photons are absorbed by the chloroplast, resulting in changes in the yields of ChlF and NPQ (Bilger *et al.*, 1995). An improved understanding of the spectral dependency of ChlF and NPQ yields is particularly important with regard to the quantitative treatment of SIF as it propagates from the leaf (van der Tol *et al.*, 2009) to the canopy in radiative transfer models (van der Tol *et al.*, 2014; Zhao *et al.*, 2016). Data collected over a wide range of species and conditions could be used to evaluate and improve the leaf-level parameterization of the ChlF emission spectrum modeled by SCOPE (van der Tol *et al.*, 2014), which is currently a linear combination of the fractional contributions of PSI and PSII derived empirically.

A formal assessment of how the nonlinear A_{net} and F_λ relationships may become increasingly linear at larger spatial scales is complicated and has yet to be performed in a quantitatively rigorous manner. Measurements such as those shown here could provide more mechanistic explanations of the linear GPP–SIF relationship observed at the satellite scale (Frankenberg *et al.*, 2011; Joiner *et al.*, 2011; Guanter *et al.*, 2012). Similar to Guanter *et al.* (2012) and Yang *et al.* (2015), where F_λ was normalized by solar zenith angle to eliminate the aPAR dependence of the SIF–GPP relationship, $\Phi F_{t,\lambda}$ could be used to improve scaling efforts and interpretations of SIF (i.e. Moya *et al.*, 2004; Louis *et al.*, 2005). Methods such as those demonstrated here under varying sun/shade and bidirectional reflectance distribution factor (BRDF) conditions linked with three-dimensional radiative transfer schemes could be used to address such questions (i.e. Hilker *et al.*, 2008).

In this study, we examined the complete ChlF emission spectrum and show small changes in F_λ beyond 800 nm, where current instruments such as the Scanning Imaging Absorption Spectrometer for Atmospheric CHartographY (SCIAMACHY) can measure SIF (Joiner *et al.*, 2016). Recently, substantial contributions to our understanding of wavelength dependencies and the potential for scaling SIF have been made by studies conducted using airborne instruments, although these studies focused primarily on the 760 and 687 nm wavelengths, suggesting that the ratio of these wavelengths can be used to infer crop stress (Rascher *et al.*, 2015; Wieneke *et al.*, 2016). Future work with instrumentation described here should examine wavelengths currently measured from spaceborne platforms (OCO-2, GOME-2, GOSAT) and investigate the ratios between red and far-red fluorescence over a range of environmental conditions and species (see reviews by Buschmann, 2007; Ač *et al.*, 2015). Moreover, a complete understanding of the ChlF emission spectrum is crucial in evaluating how red and far-red fluorescence (and their ratios) can be extrapolated in the context of future instrument development (i.e. NASA OCO-3, ESA FLEX) and SIF interpretation. Not only do studies to this end help to interpret the wavelength dependencies of SIF from spaceborne platforms, but they also provide a better understanding of how SIF magnitude varies according to time of day and environmental conditions.

Acknowledgements

We thank Dr Joseph A. Berry for insightful suggestions on the instrumental setup and experiment design and three anonymous reviewers for their helpful insights. The research was supported by a NASA Postdoctoral Program fellowship award to T.S.M., California Institute of Technology startup funds to C.F., and the Keck Institute for Space Studies. The research was carried out, in part, at the Jet Propulsion Laboratory, California Institute of Technology, under a contract with the National Aeronautics and Space Administration. California Institute of Technology. Government sponsorship is acknowledged.

Author contributions

T.S.M., C.F. and J.B.F. designed the research; T.S.M., C.F. and K.S. modified the original instrument; T.S.M., C.F., G.B.N. and T.S.D. performed the research; T.S.M. analyzed the data; T.S.M., C.F., J.B.F., Y.S., G.B.N., T.S.D., A.K. and K.S. contributed to interpretation of the analyses and writing the paper.

References

Ač A, Malenovský Z, Olejníčková J, Gallé A, Rascher U, Mohammed G. 2015. Meta-analysis assessing potential of steady-state chlorophyll fluorescence for remote sensing detection of plant water, temperature and nitrogen stress. *Remote Sensing of Environment* **168**: 420–436.

Agati G. 1998. Response of the *in vivo* chlorophyll fluorescence spectrum to environmental factors and laser excitation wavelength. A portable fibre-probe UV LED-induced fluorescence detection system. *Pure Applied Physics* **7**: 797–807.

Alonso L, Gomez-Chova L, Amoros-Lopez J, Guanter L, Calpe J. 2007. Sensitivity analysis of the FLD method for the measurement of chlorophyll fluorescence using a field spectroradiometer. *Proceedings of the 3rd International Workshop on Remote Sensing of Vegetation Fluorescence, Florence, Italy, 7–9 September 2007*.

Amorós-López J, Gomez-Chova L, Vila-Frances J, Alonso L, Calpe J, Moreno J, del Valle-Tascon S. 2008. Evaluation of remote sensing of vegetation fluorescence by the analysis of diurnal cycles. *International Journal of Remote Sensing* **29**: 5423–5436.

Anderson J, Chow W, Goodchild D. 1988. Thylakoid membrane organisation in sun/shade acclimation. *Australian Journal of Plant Physiology* **15**: 11–26.

Atherton J, Nichol CJ, Porcar-Castell A. 2016. Using spectral chlorophyll fluorescence and the photochemical reflectance index to predict physiological dynamics. *Remote Sensing of Environment* **176**: 17–30.

Baker NR. 2008. Chlorophyll fluorescence: a probe of photosynthesis *in vivo*. *Annual Review of Plant Biology* **59**: 89–113.

Bilger W, Schreiber U, Bock M. 1995. Determination of the quantum efficiency of photosystem II and of nonphotochemical quenching of chlorophyll fluorescence in the field. *Oecologia* **102**: 425–432.

Brody S, Rabinowitch E. 1957. Excitation lifetime of photosynthetic pigments *in vitro* and *in vivo*. *Science* **125**: 555–557.

Buschmann C. 2007. Variability and application of the chlorophyll fluorescence emission ratio red/far-red of leaves. *Photosynthesis Research* **92**: 261–271.

Buschmann C, Lichtenthaler HK. 1998. Principles and characteristics of multi-colour fluorescence imaging of plants. *Journal of Plant Physiology* **152**: 297–314.

Cendrero-Mateo MP, Moran MS, Papuga SA, Thorp KR, Alonso L, Moreno J, Ponce-Campos G, Rascher U, Wang G. 2016. Plant chlorophyll fluorescence: active and passive measurements at canopy and leaf scales with different nitrogen treatments. *Journal of Experimental Botany* **67**: 275–286.

Cheng Y-B, Middleton E, Zhang Q, Huemmrich K, Campbell P, Corp L, Cook B, Kustas W, Daughtry C. 2013. Integrating solar induced fluorescence and the photochemical reflectance index for estimating gross primary production in a cornfield. *Remote Sensing* **5**: 6857–6879.

Damm A, Elbers J, Erler A, Gioli B, Hamdi K, Hutjes R, Kosvancova M, Meroni M, Miglietta F, Moersch A *et al.* 2010. Remote sensing of sun-induced fluorescence to improve modeling of diurnal courses of gross primary production (GPP). *Global Change Biology* **16**: 171–186.

Drusch M, Moreno J, Del Bello U, Franco R, Goulas Y, Huth A, Kraft S, Middleton EM, Miglietta F, Mohammed G *et al.* 2016. The FLuorescence EXplorer Mission Concept – ESA's earth explorer 8. *IEEE Transactions on Geoscience and Remote Sensing* **55**: 1273–1284.

Duysens L. 1979. Transfer and trapping of excitation energy in photosystem II. In: Wolstenholme G, Fitssimons D, eds. *Chlorophyll organization and energy transfer in photosynthesis*. Amsterdam, the Netherlands: Exerpta Meidca, 323–364.

Edwards G, Baker N. 1993. Can CO_2 assimilation in maize leaves be predicted accurately from chlorophyll fluorescence analysis? *Photosynthesis Research* **37**: 89–102.

Farquhar GD, von Caemmerer S, Berry JA. 1980. A biochemical-model of photosynthetic CO_2 assimilation in leaves of C_3 species. *Planta* **149**: 78–90.

Flexas J, Escalona JM, Evain S, Gulı J, Moya I, Osmond B, Medrano H. 2002. Steady-state chlorophyll fluorescence (Fs) measurements as a tool to follow variations of net CO_2 assimilation and stomatal conductance during water-stress in C_3 plants. *Physiologia Plantarum* **114**: 231–240.

Flexas J, Escalona JM, Medrano H. 1999. Water stress induces different levels of photosynthesis and electron transport rate regulation in grapevines. *Plant, Cell & Environment* **22**: 39–48.

Flexas J, Ribas-Carbó M, Diaz-Espejo A, Galmés J, Medrano H. 2008. Mesophyll conductance to CO_2: current knowledge and future prospects. *Plant, Cell & Environment* **31**: 602–621.

Franck F, Dewez D, Popovic R. 2005. Changes in the room-temperature emission spectrum of chlorophyll during fast and slow phases of the Kautsky effect in intact leaves. *Photochemistry and Photobiology* **81**: 431–436.

Franck F, Juneau P, Popovic R. 2002. Resolution of the photosystem I and photosystem II contributions to chlorophyll fluorescence of intact leaves at room temperature. *Biochimica et Biophysica Acta – Bioenergetics* **1556**: 239–246.

Frankenberg C, Fisher JB, Worden J, Badgley G, Saatchi SS, Lee J-E, Toon GC, Butz A, Jung M, Kuze A *et al.* 2011. New global observations of the terrestrial carbon cycle from GOSAT: patterns of plant fluorescence with gross primary productivity. *Geophysical Research Letters* **38**: L17706.

Fryer M, Andrews J, Oxborough K, Blowers D, Baker N. 1998. Relationship between CO_2 assimilation, photosynthetic electron transport, and active O_2 metabolism in leaves of Maize in the field during periods of low temperature. *Plant Physiology* **116**: 571–580.

Gamon JA, Field CB, Bilger W, Bjrkman O, Fredeen AL, Penuelas J. 1990. Remote sensing of the xanthophyll cycle and chlorophyll fluorescence in sunflower leaves and canopies. *Oecologia* **85**: 1–7.

Genty B, Briantais J-M, Baker NR. 1989. The relationship between the quantum yield of photosynthetic electron transport and quenching of chlorophyll fluorescence. *Biochimica et Biophysica Acta (BBA) – General Subjects* **990**: 87–92.

Genty B, Wonders J, Baker NR. 1990. Non-photochemical quenching of Fo in leaves is emission wavelength dependent: consequences for quenching analysis and its interpretation. *Photosynthesis Research* **26**: 133–139.

Gitelson AA, Buschmann C, Lichtenthaler HK. 1998. Leaf chlorophyll fluorescence corrected for re-absorption by means of absorption and reflectance measurements. *Journal of Plant Physiology* **152**: 283–296.

Govindjee . 1995. Sixty-three years since Kautsky: chlorophyll a fluorescence. *Australian Journal of Plant Physiology* **22**: 131–160.

Guanter L, Alonso L, Gómez-Chova L, Amórós-Lopez J, Vila J, Moreno J. 2007. Estimation of solar-induced vegetation fluorescence from space measurements. *Geophysical Research Letters* **34**: L08401.

Guanter L, Frankenberg C, Dudhia A, Lewis PE, Gómez-Dans J, Kuze A, Suto H, Grainger RG. 2012. Retrieval and global assessment of terrestrial chlorophyll fluorescence from GOSAT space measurements. *Remote Sensing of Environment* **121**: 236–251.

Guanter L, Zhang Y, Jung M, Joiner J, Voigt M, Berry JA, Frankenberg C, Huete AR, Zarco-Tejada P, Lee J-E *et al.* 2014. Global and time-resolved monitoring of crop photosynthesis with chlorophyll fluorescence. *Proceedings of the National Academy of Sciences, USA* **111**: E1327–E1333.

Hasegawa M, Shiina T, Terazima M, Kumazaki S. 2010. Selective excitation of photosystems in chloroplasts inside plant leaves observed by near-infrared laser-based fluorescence spectral microscopy. *Plant and Cell Physiology* **51**: 225–238.

Hilker T, Coops NC, Hall FG, Black TA, Wulder MA, Nesic Z, Krishnan P. 2008. Separating physiologically and directionally induced changes in PRI using BRDF models. *Remote Sensing of Environment* **112**: 2777–2788.

Joiner J, Guanter L, Lindstrot R, Voigt M, Vasilkov AP, Middleton EM, Huemmrich KF, Yoshida Y, Frankenberg C. 2013. Global monitoring of terrestrial chlorophyll fluorescence from moderate-spectral-resolution near-infrared satellite measurements: methodology, simulations, and application to GOME-2. *Atmospheric Measurement Techniques* **6**: 2803–2823.

Joiner J, Yoshida Y, Guanter L, Middleton EM. 2016. New methods for retrieval of chlorophyll red fluorescence from hyper-spectral satellite instruments: simulations and application to GOME-2 and SCIAMACHY. *Atmospheric Measurement Techniques Discussions* **9**: 3939–3967.

Joiner J, Yoshida Y, Vasilkov AP, Corp LA, Middleton EM. 2011. First observations of global and seasonal terrestrial chlorophyll fluorescence from space. *Biogeosciences* **8**: 637–651.

Kalaji HM, Schansker G, Ladle RJ, Goltsev V, Bosa K, Allakhverdiev SI, Brestic M, Bussotti F, Calatayud A, Dąbrowski P *et al.* 2014. Frequently asked

questions about *in vivo* chlorophyll fluorescence: practical issues. *Photosynthesis Research* **122**: 121–158.

Kautsky H, Hirsch A. 1931. Neue Versuche zur Kohlensäureassimilation. *Naturwissenschaften* **19**: 964.

Kitajima K, Butler WL. 1975. Quenching of chlorophyll fluorescence and primary photochemistry in chloroplasts by dibromothymoquinone. *Biochimica et Biophysica Acta (BBA) – Bioenergetics* **376**: 105–115.

Krause GH, Weis E. 1991. Chlorophyll fluorescence and photosynthesis: the basics. *Annual Review of Plant Physiology and Plant Molecular Biology* **42**: 313–349.

Lambrev PH, Nilkens M, Miloslavina Y, Jahns P, Holzwarth AR. 2010. Kinetic and spectral resolution of multiple nonphotochemical quenching components in Arabidopsis leaves. *Plant Physiology* **152**: 1611–1624.

Lichtenthaler HK, Wenzel O, Buschmann C, Gitelson A. 1998. Plant stress detection by reflectance and fluorescence. *Annals of the New York Academy of Sciences* **851**: 271–285.

Logan BA, Adams WW, Demmig-Adams B. 2007. Viewpoint: avoiding common pitfalls of chlorophyll fluorescence analysis under field conditions. *Functional Plant Biology* **34**: 853.

Long SP, Bernacchi CJ. 2003. Gas exchange measurements, what can they tell us about the underlying limitations to photosynthesis? Procedures and sources of error. *Journal of Experimental Botany* **54**: 2393–2401.

Louis J, Ounis A, Ducruet JM, Evain S, Laurila T, Thum T, Aurela M, Wingsle G, Alonso L, Pedros R *et al.* 2005. Remote sensing of sunlight-induced chlorophyll fluorescence and reflectance of Scots pine in the boreal forest during spring recovery. *Remote Sensing of Environment* **96**: 37–48.

Magney TS, Eusden SA, Eitel JUH, Logan BA, Jiang J, Vierling LA. 2014. Assessing leaf photoprotective mechanisms using terrestrial LiDAR: towards mapping canopy photosynthetic performance in three dimensions. *New Phytologist* **201**: 344–356.

Magney TS, Logan BA, Reblin JR, Griffin KL, Boelman NB, Eitel JUH, Prager C, Greaves H, Vierling LA. 2017. Xanthophyll cycle activity in two prominent Arctic shrub species. *Arctic, Antarctic, and Alpine Research* **49**: 277–289.

Maxwell K, Johnson GN. 2000. Chlorophyll fluorescence – a practical guide. *Journal of Experimental Botany* **51**: 659–668.

Meroni M, Colombo R. 2006. Leaf level detection of solar induced chlorophyll fluorescence by means of a subnanometer resolution spectroradiometer. *Remote Sensing of Environment* **103**: 438–448.

Meroni M, Rossini M, Guanter L, Alonso L, Rascher U, Colombo R, Moreno J. 2009. Remote sensing of solar-induced chlorophyll fluorescence: review of methods and applications. *Remote Sensing of Environment* **113**: 2037–2051.

Meroni M, Rossini M, Picchi V, Panigada C, Cogliati S, Nali C, Colombo R. 2008. Assessing steady-state fluorescence and PRI from hyperspectral proximal sensing as early indicators of plant stress: the case of ozone exposure. *Sensors* **8**: 1740–1754.

Moya I, Camenen L, Evain S, Goulas Y, Cerovic ZG, Latouche G, Flexas J, Ounis A. 2004. A new instrument for passive remote sensing: 1. Measurements of sunlight-induced chlorophyll fluorescence. *Remote Sensing of Environment* **91**: 186–197.

Murchie EH, Lawson T. 2013. Chlorophyll fluorescence analysis: a guide to good practice and understanding some new applications. *Journal of Experimental Botany* **64**: 3983–3998.

Pedrós R, Moya I, Goulas Y, Jacquemoud S. 2008. Chlorophyll fluorescence emission spectrum inside a leaf. *Photochemical & Photobiological Sciences* **7**: 498–502.

Pérez-Priego O, Zarco-Tejada PJ, Miller JR, Sepulcre-Cantó G, Fereres E. 2005. Detection of water stress in orchard trees with a high-resolution spectrometer through chlorophyll fluorescence in-filling of the O_2-A band. *IEEE Transactions on Geoscience and Remote Sensing* **43**: 2860–2868.

Pfundel EE. 1998. Estimating the contribution of photosystem I to total leaf chlorophyll fluorescence. *Photosynthesis Research* **56**: 185–195.

Plascyk JA, Gabriel FC. 1975. The Fraunhofer line discriminator MKII an airborne instrument for precise and standardized ecological luminescence measurement. *IEEE Transactions on Instrumentation and Measurement* **24**: 306–313.

Porcar-Castell A, Tyystjarvi E, Atherton J, van der Tol C, Flexas J, Pfundel EE, Moreno J, Frankenberg C, Berry JA. 2014. Linking chlorophyll α fluorescence to photosynthesis for remote sensing applications: mechanisms and challenges. *Journal of Experimental Botany* **65**: 4065–4095.

Rappaport F, Béal D, Joliot A, Joliot P. 2007. On the advantages of using green light to study fluorescence yield changes in leaves. *Biochimica et Biophysica Acta – Bioenergetics* **1767**: 56–65.

Rascher U, Agati G, Alonso L, Cecchi G, Champagne S, Colombo R, Damm A, Daumard F, Kosvancova M, Lognoli D *et al.* 2009. CEFLES2: the remote sensing component to quantify photosynthetic efficiency from the leaf to the region by measuring sun-induced fluorescence in the oxygen absorption bands. *Biogeosciences* **6**: 1181–1198.

Rascher U, Alonso L, Burkart A, Cilia C, Cogliati S, Colombo R, Damm A, Drusch M, Guanter L, Hanus J *et al.* 2015. Sun-induced fluorescence – a new probe of photosynthesis: first maps from the imaging spectrometer HyPlant. *Global Change Biology* **21**: 4673–4684.

Schansker G, Tóth SZ, Strasser RJ. 2006. Dark recovery of the Chl *a* fluorescence transient (OJIP) after light adaptation: the q*T*-component of non-photochemical quenching is related to an activated photosystem I acceptor side. *Biochimica et Biophysica Acta – Bioenergetics* **1757**: 787–797.

van der Tol C, Berry JA, Campbell P, Rascher U. 2014. Models of fluorescence and photosynthesis for interpreting measurements of solar-induced chlorophyll fluorescence. *Journal of Geophysical Research: Biogeosciences* **119**: 2312–2327.

van der Tol C, Verhoef W, Rosema A. 2009. A model for chlorophyll fluorescence and photosynthesis at leaf scale. *Agricultural and Forest Meteorology* **149**: 96–105.

Tubuxin B, Rahimzadeh-Bajgiran P, Ginnan Y, Hosoi F, Omasa K. 2015. Estimating chlorophyll content and photochemical yield of photosystem II (φPSII) using solar-induced chlorophyll fluorescence measurements at different growing stages of attached leaves. *Journal of Experimental Botany* **66**: 5595–5603.

Van Wittenberghe S, Alonso L, Verrelst J, Hermans I, Valcke R, Veroustraete F, Moreno J, Samson R. 2014. A field study on solar-induced chlorophyll fluorescence and pigment parameters along a vertical canopy gradient of four tree species in an urban environment. *Science of the Total Environment* **466–467**: 185–194.

Van Wittenberghe S, Alonso L, Verrelst J, Moreno J, Samson R. 2015. Bidirectional sun-induced chlorophyll fluorescence emission is influenced by leaf structure and light scattering properties – a bottom-up approach. *Remote Sensing of Environment* **158**: 169–179.

Verma M, Schimel D, Evans B, Frankenberg C, Beringer J, Drewry D, Magney T, Marang I, Hutley L, Moore C *et al.* 2017. Effect of environmental conditions on the relationship between solar-induced fluorescence and gross primary productivity at an OzFlux grassland site. *Journal of Geophysical Research – Biogeosciences* **122**: 716–733.

Vilfan N, van der Tol C, Muller O, Rascher U, Verhoef W. 2016. Fluspect-B: a model for leaf fluorescence, reflectance and transmittance spectra. *Remote Sensing of Environment* **186**: 596–615.

Vogelmann TC. 1993. Plant tissue optics. *Annual Review of Plant Physiology Plant Molecular Biology* **44**: 231–251.

Vogelmann TC, Evans JR. 2002. Profiles of light absorption and chlorophyll within spinach leaces from chlorophyll fluorescence. *Plant, Cell & Environment* **25**: 1313–1323.

Walther S, Voigt M, Thum T, Gonsamo A, Zhang Y, Koehler P, Jung M, Varlagin A, Guanter L. 2015. Satellite chlorophyll fluorescence measurements reveal large-scale decoupling of photosynthesis and greenness dynamics in boreal evergreen forests. *Global Change Biology* **22**: 2979–2996.

Wieneke S, Ahrends H, Damm A, Pinto F, Stadler A, Rossini M, Rascher U. 2016. Airborne based spectroscopy of red and far-red sun-induced chlorophyll fluorescence: implications for improved estimates of gross primary productivity. *Remote Sensing of Environment* **184**: 664–667.

Wood JD, Griffis TJ, Baker JM, Frankenberg C, Verma M, Yuen K. 2016. Multi-scale analyses reveal robust relationships between gross primary production and solar induced fluorescence. *Geophysical Research Letters* **44**: 533–541.

Yang X, Tang J, Mustard JF, Lee J, Rossini M, Joiner J, Munger JW, Kornfeld A, Richardson AD. 2015. Solar-induced chlorophyll fluorescence that correlates with canopy photosynthesis on diurnal and seasonal scales in a temperate deciduous forest. *Geophysical Research Letters* **42**: 2977–2987.

Zarco-Tejada PJ, González-Dugo V, Berni JAJ. 2012. Fluorescence, temperature and narrow-band indices acquired from a UAV platform for water stress detection using a micro-hyperspectral imager and a thermal camera. *Remote Sensing of Environment* **117**: 322–337.

Zarco-Tejada PJ, Morales A, Testi L, Villalobos FJ. 2013. Spatio-temporal patterns of chlorophyll fluorescence and physiological and structural indices acquired from hyperspectral imagery as compared with carbon fluxes measured with eddy covariance. *Remote Sensing of Environment* **133**: 102–115.

Zarco-Tejada PJ, Pushnik JC, Dobrowski S, Ustin SL. 2003. Steady-state chlorophyll a fluorescence detection from canopy derivative reflectance and double-peak red-edge effects. *Remote Sensing of Environment* **84**: 283–294.

Zhao F, Dai X, Verhoef W, Guo Y, van der Tol C, Li Y, Huang Y. 2016. FluorWPS: a Monte Carlo ray-tracing model to compute sun-induced chlorophyll fluorescence of three-dimensional canopy. *Remote Sensing of Environment* **187**: 385–399.

Supporting Information

Additional Supporting Information may be found online in the Supporting Information tab for this article:

Fig. S1 Example spectra from 450 to 850 nm to demonstrate derivation of maximum spectral fluorescence ($F_{m,\lambda}$) and steady-state fluorescence (F_λ) from initial saturating pulse, actinic light, and the modulating light ($F_{ML,\lambda}$) for both species and conditions.

Fig. S2 Light response curves for net photosynthesis (A_{net}) and stomatal conductance (g_s) for both species and conditions.

Fig. S3 Complete time series of four example spectra showing steady-state spectral fluorescence (F_λ), spectral fluorescence yield ($\Phi F_{t,\lambda}$), and maximum spectral fluorescence ($F_{m,\lambda}$) overlaid with transient fluorescence intensity (F_t) and maximum fluorescence (F_m) from pulse-amplitude modulation (PAM) for both species and conditions during a light response curve.

Fig. S4 Conceptual figure showing the derivation of spectral fluorescence emission ($F_{m,\lambda}$) from the modulating light ($F_{ML,\lambda}$).

Fig. S5 Relationship between transient fluorescence (F_t) derived from pulse-amplitude modulation (PAM) and from spectral fluorescence from the modulating light ($F_{ML,\lambda}$).

Fig. S6 Conceptual figure expanding Fig. 2, highlighting the derivation of all spectral fluorescence parameters (F_λ) and pulse-amplitude modulation (PAM) parameters during the full first 14 min of a light response curve.

Fig. S7 Relative differences in spectral fluorescence (F_λ) emission curves separated by both species and conditions.

Table S1 Nomenclature for additional parameters from pulse-amplitude modulation (PAM) fluorescence and spectrally derived fluorescence

Please note: Wiley Blackwell are not responsible for the content or functionality of any Supporting Information supplied by the authors. Any queries (other than missing material) should be directed to the *New Phytologist* Central Office.